Journal of Solid State Chemistry **150,** 81–95 (2000)
doi:10.1006/jssc.1999.8550, available online at http://www.idealibrary.com on IDEAL®

Crystal Structure and Thermal Behavior of $La(H_2O)_2M(C_2O_4)_2 \cdot H_2O$ (M = K, NH_4) Studied by Powder X-Ray Diffraction

T. Bataille, M. Louër, J.-P. Auffrédic, and D. Louër

Laboratoire de Chimie du Solide et Inorganique Moléculaire (UMR CNRS 6511), Université de Rennes I, Avenue du Général Leclerc, 35042 Rennes Cedex, France

Received July 22, 1999; in revised form October 6, 1999; accepted October 22, 1999

The crystal structure of $La(H_2O)_2K(C_2O_4)_2 \cdot H_2O$ has been solved *ab initio* from powder diffraction data collected with conventional monochromatic X-rays. The symmetry is monoclinic, space group $C2/m$, cell dimensions $a = 22.033(1)$ Å, $b = 7.6003(5)$ Å, $c = 6.6418(4)$ Å, $\beta = 103.814(6)^\circ$, $V = 1080.05(8)$ Å^3, $Z = 4$. Since a disorder of one oxalate group is observed with all possible monoclinic space groups, it has been found convenient to describe the crystal structure in a triclinic subcell. The disorder problem is thoroughly discussed with respect to the powder diffraction data available for this material. From this description the compound exhibits a layered-type structure, which could explain reported cation-exchange properties. The layers are formed by four-membered rings $[La(C_2O_4)]_4$. The potassium atom and two of the three water molecules are located between the layers. The third water molecule lies on the layer in tunnels with a diamond-shaped cross section. The lanthanum atom is tenfold-coordinated in a distorted bicapped square antiprism and the potassium atom is eightfold-coordinated in a dodecahedron. The crystal structure of $La(H_2O)_2(NH_4)(C_2O_4)_2 \cdot H_2O$ is isostructural with that of $La(H_2O)_2K(C_2O_4)_2 \cdot H_2O$ [$a = 22.130(4)$ Å, $b = 7.774(1)$ Å, $c = 6.655(2)$ Å, $\beta = 105.28(2)^\circ$, $V = 1104.4(3)$ Å^3]. The thermal decomposition of these two precursors has been carried out by means of temperature-dependent X-ray diffraction and TG-DSC. The dehydration leads to anhydrous phases, which are amorphous and poorly crystalline for the potassium and ammonium compounds, respectively. Amorphous $LaK(C_2O_4)_2$ crystallizes at 260°C. Its symmetry is monoclinic with the cell dimensions $a = 5.687(3)$ Å, $b = 15.241(5)$ Å, $c = 9.017(4)$ Å, $\beta = 92.82(3)^\circ$. At higher temperature, the decomposition of $LaK(C_2O_4)_2$ yields $La_2O_2CO_3$ (Type-Ia), $La_2O_2CO_3$ (Type-II), and pure La_2O_3, successively. $La(NH_4)(C_2O_4)_2$ leads to $La_2O_2CO_3$ (Type-II) and, finally, La_2O_3.

INTRODUCTION

There is an increasing interest in lanthanide carboxylates for their ability to form porous open-framework materials having attractive topologies (1–4). The use of the most common oxalate ligand in these compounds has often provided examples of interesting materials with zeolitic properties (5 and references therein) or with host–guest shapes (6). Recently, such properties were extended to the mixed compound $YK(C_2O_4)_2 \cdot 4H_2O$ (7), in which a nanoporous framework with zeolitic water molecules was clearly pointed out from X-ray powder diffraction data. Similarly to other families of compounds (see, for example, Ref. (8)), the spectacular advances in powder diffraction methodology (9) can be applied to shed light on the crystal chemistry of the oxalate compounds obtained only in a microcrystalline form. In this respect the mixed yttrium potassium oxalate with a three-dimensional open-crystal structure (7) is a representative example. Following our studies on mixed lanthanum or yttrium oxalates, recently we have demonstrated that the chemically related yttrium sodium oxalate (10) has, surprisingly, a layered-type crystal structure. This change of dimensionality in the crystal structure of a member of this oxalate family has motivated the present study, which is an extension to mixed lanthanum oxalates containing potassium or ammonium. The present contribution deals with the synthesis of lanthanum potassium oxalate and its related ammonium phase, their crystal structure determined *ab initio* from powder diffraction data collected with a conventional X-ray source, and the thermal behavior of these compounds. Although no structural data have been reported for these phases, interesting cation-exchange properties were described recently for the ammonium phase and applied in nuclear technology (11–13). Indeed, it has been shown that ammonium groups can be exchanged, with a high yield, by U(IV) and Th. These features are of importance in the enrichment processes based on the separation of the two main oxidation states of uranium (11) and, also, on the extraction of thorium (12, 13) in nuclear wastes. In order to explain these noteworthy properties the crystal structure of the ammonium phase is clearly needed. The present study will also contribute to explanations of this interesting behavior of the ammonium phase.

0022-4596/00 $35.00

EXPERIMENTAL

1. Material Preparation

$La(H_2O)_2M(C_2O_4)_2 \cdot H_2O$ ($M = K$, NH_4) was synthesized from concentrated solutions to avoid the precipitation of lanthanum oxalate, $La_2(C_2O_4)_3 \cdot 10H_2O$, which occurs when diluted solutions are used. Two millimole of lanthanum nitrate hexahydrate (Aldrich, No. 33,193-7) and 5 mmol of oxalic acid dihydrate (Prolabo, rectapur No. 20558.365) were dissolved in 20 ml concentrated nitric acid (Merck A.R. 65%). Concentrated solutions of potassium hydroxide or ammonia were added dropwise until the precipitation of the mixed potassium or ammonium compounds was complete and the pH of the solutions was increased to 8. Since the reaction is exothermic, the precipitates were filtered off while hot, to avoid the formation of potassium nitrate or ammonium nitrate, and were dried at room temperature. Only microcrystalline powders were obtained from these syntheses. Attempts to grow a single crystal under hydrothermal conditions were unsuccessful. The La : K ratio (1 : 1) was determined by energy dispersive spectrometry (EDS) and the chemical formulae of the two compounds were confirmed from thermogravimetry (TG) and the crystal structure determinations. The synthesis method applied here presents similarities with those reported long ago for the preparation of double ammonium oxalates of rare earths (14). In the previous work, the compounds were also obtained in powder form and only a rough characterization from X-ray powder diffraction was reported.

2. Collection of High Resolution Powder X-Ray Diffraction Data

High-quality powder diffraction data for $La(H_2O)_2K(C_2O_4)_2 \cdot H_2O$ and $La(H_2O)_2(NH_4)(C_2O_4)_2 \cdot H_2O$ were obtained with a Siemens D500 diffractometer using monochromatic Cu$K\alpha_1$ radiation ($\lambda = 1.5406$ Å), selected with an incident beam curved crystal germanium monochromator, with the parafocusing Bragg–Brentano geometry. The instrumental resolution function (IRF) of the setup exhibits a shallow minimum of 0.065° (2θ) at about 40° (2θ) and has twice the value at about 130° (2θ). The powders were mounted in a top-loaded sample holder (15) to minimize preferred orientation effects. The pattern of $La(H_2O)_2K(C_2O_4)_2 \cdot H_2O$ was scanned over the angular range 10–130° (2θ) with a step length of 0.02° (2θ) and a counting time of 40 s step^{-1} until 70° (2θ) and 80 s step^{-1} from 70.02° (2θ) to the end of the scan. The second range was then scaled to a counting time of 40 s step^{-1}. The pattern of $La(H_2O)_2(NH_4)(C_2O_4)_2 \cdot H_2O$ was scanned over the range 7–95° (2θ), with a step length of 0.02° (2θ), counting times of 30 s step^{-1} from 7° (2θ) to 33° (2θ) and 60 s step^{-1} from 33.02° (2θ) to the end of the scan. The full pattern was scaled to a counting time of 30 s step^{-1}. After data collection, the stability of the X-ray source was checked by recording again the diffraction lines at low angles. In order to estimate the presence of preferred orientation effects in the data set collected with the reflection geometry, two additional powder diffraction data were collected using the Debye–Scherrer geometry with monochromatic Cu$K\alpha_1$ radiation, using a Bruker AXS D5005 diffractometer and the curved position sensitive detector (PSD) from INEL. In both cases, the sample was sealed in a 0.3-mm capillary. Figure 1 shows that the data collected using the Bragg–Brentano geometry display a slight orientation effect in the direction perpendicular to (*hk*0). Precise powder diffraction data at nonambient temperature were collected for the anhydrous oxalates in an isothermal mode with a Bruker AXS D5005 diffractometer, using Cu$K\alpha$ radiation ($\lambda K\alpha_1 = 1.5406$ Å, $\lambda K\alpha_2 = 1.5444$ Å), selected with a diffracted-beam graphite monochromator. The samples were placed in an Anton Paar HTK1200 high-temperature oven-camera.

The extraction of the peak positions of the patterns was performed with the Socabim fitting program PROFILE, available in the software package DIFFRAC-AT supplied by Siemens. Patterns indexing was carried out with the program DICVOL91 (16). The programs EXPO (17) and SHELX-97 (18) were used for structure solutions, and FULLPROF (19) was used for the refinement of the structures by the Rietveld method. The programs POWDER CELL 1.0 (20), DIAMOND 2.1, and WebLab ViewerLite supplied by Molecular Simulations Inc. were used for structure drawings.

3. Thermal Analyses

Temperature-dependent X-ray diffraction (TDXD) was performed with a powder diffractometer combining the PSD (CPS120) from INEL and a high-temperature attachment from Rigaku. The detector was used in a semifocusing geometry by reflection with the monochromatic Cu$K\alpha_1$ radiation, as described elsewhere (21). In this geometry the flat sample is stationary. An angle of 6° between the incident beam and the surface of the sample was selected. The thermal decomposition of $La(H_2O)_2K(C_2O_4)_2 \cdot H_2O$ was carried out under flowing nitrogen and that of $La(H_2O)_2(NH_4)(C_2O_4)_2 \cdot H_2O$ under flowing air.

TG-DSC measurements were performed with a Rigaku Thermoflex instrument under flowing nitrogen or air. For TG analyses only, the powdered samples were spread evenly in a large platinum crucible to avoid mass effects.

STRUCTURE DETERMINATION OF $La(H_2O)_2M(C_2O_4)_2 \cdot H_2O$ (M = K, NH_4)

1. Pattern Indexing

$La(H_2O)_2K(C_2O_4)_2 \cdot H_2O$. The first 29 lines of the X-ray powder diffraction pattern were indexed with an absolute

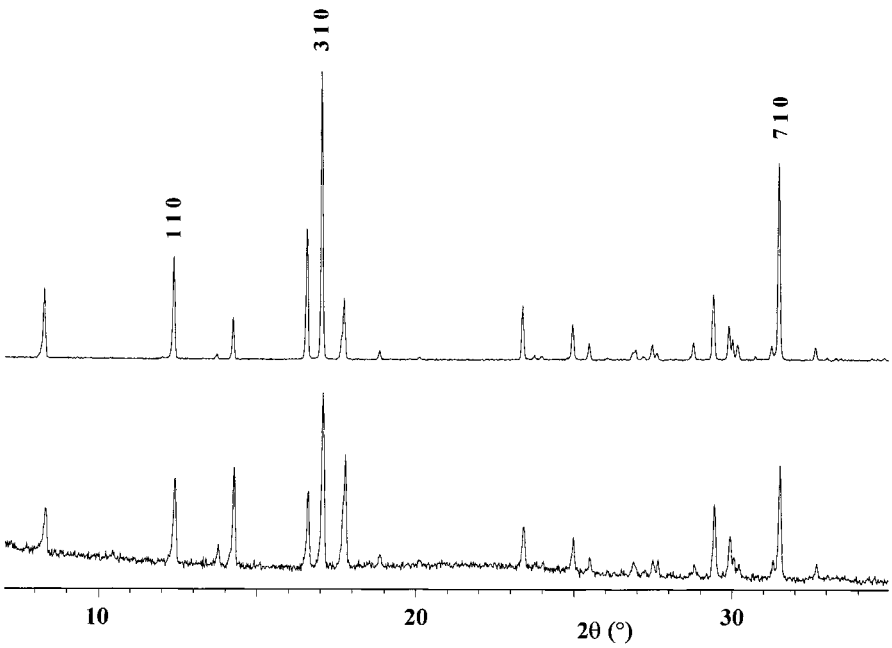

FIG. 1. Parts of the powder diffraction data of $La(H_2O)_2K(C_2O_4)_2 \cdot H_2O$ collected with the Bragg–Brentano geometry (top) and with the Debye–Scherrer geometry (bottom).

error of 0.03° (2θ) on the peak positions, on the basis of a monoclinic solution with the figures of merit $M_{29} = 35$ and $F_{29} = 84(0.005, 77)$. A least-squares refinement from the resolved diffraction lines available led to the unit cell dimensions $a = 22.033(1)$ Å, $b = 7.6003(5)$ Å, $c = 6.6418(4)$ Å, $\beta = 103.814(6)°$, and $V = 1080.05(8)$ Å^3. According to the absent reflections, the most likely space groups were $C2$, Cm, and $C2/m$ [$M_{20} = 82$, $F_{30} = 145(0.004,47)$]. The powder data have been submitted to the ICDD (22) for possible inclusion in the Powder Diffraction File.

$La(H_2O)_2(NH_4)(C_2O_4)_2 \cdot H_2O$. The indexing of the first 25 lines of the pattern gave a monoclinic cell similar to the cell obtained for the potassium compound, with $M_{25} = 25$ and $F_{25} = 57(0.006,69)$. The refinement of the unit cell parameters was carried out with the complete set of resolved diffraction lines available. The unit cell dimensions were $a = 22.130(4)$ Å, $b = 7.774(1)$ Å, $c = 6.655(2)$ Å, $\beta = 105.28(2)°$, and $V = 1104.4(3)$ Å^3, S.G. $C2$, Cm, or $C2/m$ [$M_{20} = 45$ and $F_{30} = 72(0.009,47)$]. The powder data have been submitted to the ICDD (22) for possible inclusion in the Powder Diffraction File.

2. *Ab Initio Structure Determination of $La(H_2O)_2K(C_2O_4)_2 \cdot H_2O$*

Integrated intensities were extracted with the program EXPO in the angular range 10–65° (2θ). Among the 218 reflections obtained, 121 were considered as statistically independent, according to the degree of diffraction-line overlap (23). The structure-factor amplitudes thus obtained were used, with space group $C2/m$, for the structure solution carried out with the direct-methods program available in the software package. A partial model corresponding to the lowest residual value $R = 0.11$ was displayed, including La, K, three oxalate oxygen atoms, two carbon atoms, and two water molecules in the asymmetric unit. The model corresponded to the general formula "$LaK(C_2O_4)_{1.5} \cdot 2H_2O$," and one carbon atom lying in a special position (multiplicity of $\frac{1}{2}$) was needed to complete the amount of expected oxalates. The atomic coordinates generated by the program EXPO were used in the program SHELXL-97. A difference Fourier calculation showed only one possible C atom, namely, C3, lying in a general position, and two additional peaks (O31, O32) in the vicinity of C3, as shown in Fig. 2. Note that the center of the oxalate group is on the inversion center ($\frac{1}{4}$, $\frac{1}{4}$, 0). Although the number of oxygen atoms in the unit cell is thus correct, it is clear that the number of oxalates exceeds the amount of expected oxalate groups. Such a model is misleading, since O31 lies in the mirror plane and generates an infinite chain along the b axis. It is obvious that a disorder exists along this axis between this oxalate group and the third water molecule. Indeed, after the removal of half the C3 atoms, O32 can be considered as either an oxalate oxygen atom or a water molecule. However, in view of the quality of the data available, it appeared not reasonable to consider a supercell in order to overcome this disorder problem. Nevertheless, attempts were made to

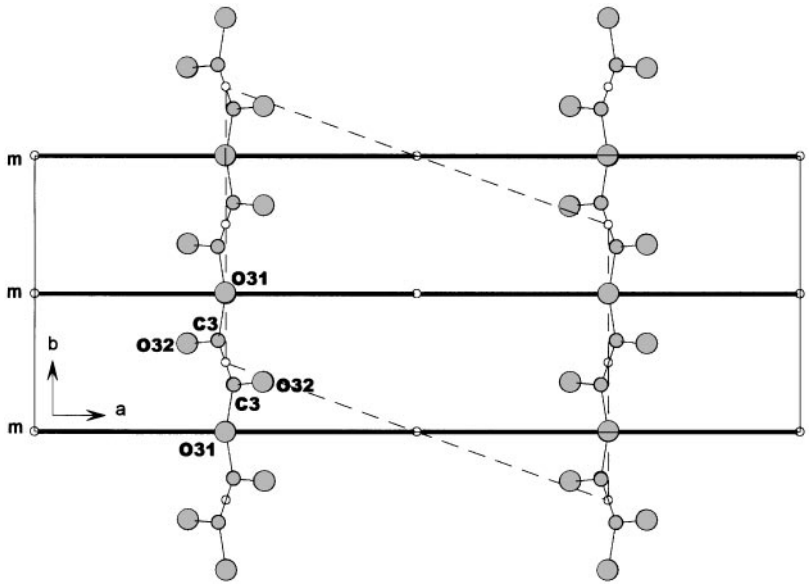

FIG. 2. The C3, O31, and O32 atoms corresponding to the three peaks displayed on the last difference Fourier map. The cell in the dotted line is the triclinic subcell.

solve the structure in space groups with no mirror planes, i.e., $C2$ and also $P2_1/a$, though the last is not C-centered. In all cases it was still necessary to exceed the number of C atoms to complete the last oxalate group. At this stage, it was clear that nothing more could be done in the monoclinic symmetry. It must be noted here that the structure determination strategy was carried out similarly from the two (preferred-orientation-free) data sets collected with the Debye–Scherrer geometry. The same conclusions were obtained. Then, for the structure description it appeared suitable to consider the triclinic subcell, S.G. $P\bar{1}$, in order to preserve the center of symmetry, which is necessary to link C3 to its symmetry equivalent as shown in Fig. 2. This cell is derived from the transformation matrix $[\frac{1}{2}, -\frac{1}{2}, 0/0, 1, 0/0, 0, 1]$ applied to the base vectors of the C-centered monoclinic cell. The new set of unit cell parameters is $a' = 11.654$ Å, $b' = 7.6003$ Å, $c' = 6.6418$ Å, $\alpha' = 90.0°$, $\beta' = 103.05°$, $\gamma' = 109.03°$, $V' = 540.02$ Å^3, space group $P\bar{1}$. The structure was solved again in this triclinic cell by the Patterson method and the direct methods by means of the program SHELXS-97, from which the complete model was thus displayed by means of difference Fourier calculations. A least-squares Rietveld refinement with the program FULLPROF was carried out in the angular range 10–130° (2θ) containing 1832 reflections. A pseudo-Voigt function was used to describe line profiles, with a variation of the mixing factor η as a linear function of the 2θ angle. The refinement involved 51 atomic parameters, 1 scale factor, 1 overall isotropic displacement parameter, 1 zero point, 6 cell parameters, 3 half-widths, 4 line asymmetry parameters, and 5 background polynomial parameters. In addition, one preferred orientation parameter was refined in the direction of the diffraction vector perpendicular to ($hk0$), in agreement with the experimental observation displayed in Fig. 1 and with the layered structure discussed below. Soft constraints were applied on distances within the oxalate groups, i.e., the bond lengths were restrained to 1.250(12) Å for C–O and 1.530(12) Å for C–C, as usually observed in the literature [see, for instance, Refs (5, 7, 10)]. The final refinement converged to the residual factors $R_F = 0.097$ and $R_{wp} = 0.109$. Crystallographic data and details of the Rietveld refinement are given in Table 1. Final atomic coordinates in the triclinic subcell are given in Table 2. The atomic coordinates can be transformed in the C-centered monoclinic cell according to the transpose of the transformation matrix given previously, $[\frac{1}{2}, 0, 0/-\frac{1}{2}, 1, 0/0, 0, 1]$ and a translation of $[\frac{1}{4}, \frac{1}{4}, 0]$ (the origin of the triclinic cell is the center of Ox3, see Fig. 2). The initial atomic positions displayed by the program EXPO are thus retrieved. Apart from atoms lying in special positions in the space group $C2/m$, two independent sets of atoms in two adjacent triclinic subcells are obviously needed to obtain the complete model in the monoclinic cell, which contains eight symmetry-equivalent positions. As shown in Table 2, these sets are found in the triclinic structure solution, except that: (i) only one set of C3 atoms is displayed (the second set was not observed in the difference Fourier map); (ii) O32 and Ow3 lead to the same symmetry-equivalent positions in the monoclinic cell. A site occupancy factor of $\frac{1}{2}$ is then necessary for atoms C3, O32, and Ow3 in the monoclinic cell. It is obvious that these three light atoms were the source of the disorder observed previously. It can be noted that a Rietveld

TABLE 1
Crystallographic Data and Details of the Rietveld Refinements for $La(H_2O)_2K(C_2O_4)_2 \cdot H_2O$ and $La(H_2O)_2(NH_4)(C_2O_4)_2 \cdot H_2O$ (Triclinic Subcells, S. G. $P\bar{1}$)

	$La(H_2O)_2K(C_2O_4)_2 \cdot H_2O$	$La(H_2O)_2(NH_4)(C_2O_4)_2 \cdot H_2O$
Z	2	2
Wavelength (Å)	1.5406	1.5406
2θ range (°)	10–130	7–95
No. of atoms	17	17
No. of reflections	1832	1020
No. of structural parameters	53	53
No. of profile parameters	22	22
R_F	0.097	0.059
R_B	0.162	0.130
R_p	0.078	0.095
R_{wp}	0.109	0.135
R_{exp}	0.060	0.062

refinement using the program FULLPROF, carried out in the full angular range on the basis of the new positions in the monoclinic cell, led to quite similar results ($R_F = 0.111$ and $R_{wp} = 0.120$). The atomic coordinates refined in the monoclinic cell are given in Table 2. Figure 3 shows the best agreement obtained between calculated and observed patterns for the triclinic cell. Selected bonds and angles in the triclinic cell are listed in Table 3. In the subsequent text, the structure will be described in the triclinic cell, which does not imply any disorder, although the actual symmetry of $La(H_2O)_2K(C_2O_4)_2 \cdot H_2O$ can be definitely considered as monoclinic.

3. *Structure Refinement of $La(H_2O)_2(NH_4)(C_2O_4)_2 \cdot H_2O$*

The set of atomic coordinates obtained from the structure determination of $La(H_2O)_2K(C_2O_4)_2 \cdot H_2O$ in the triclinic subcell was used in the refinement of the structure of $La(H_2O)_2(NH_4)(C_2O_4)_2 \cdot H_2O$, except that K was replaced by the nitrogen atom of the ammonium group. The least-squares Rietveld refinement was carried out with the program FULLPROF in the angular range 7–95° (2θ) containing 1020 reflections. Distances within the oxalate groups were restrained to 1.25(2) Å for C–O and 1.53(2) Å for C–C. The final refinement converged to the residual factors $R_F = 0.059$ and $R_{wp} = 0.135$. Crystallographic data and details of the Rietveld refinement are given in Table 1. Similarly to the discussion reported for $La(H_2O)_2K(C_2O_4)_2 \cdot H_2O$, the atomic coordinates of $La(H_2O)_2(NH_4)(C_2O_4)_2 \cdot H_2O$ can be transformed in the monoclinic cell. A Rietveld refinement in the monoclinic cell, carried out

TABLE 2
Fractional Atomic Coordinates for $La(H_2O)_2K(C_2O_4)_2 \cdot H_2O$ in the Triclinic Subcell (S.G. $P\bar{1}$) and the Monoclinic Cell (S.G. $C2/m$) (S_{occ}: site occupancy factor)

	$P\bar{1}$			$C2/m$			
	x	y	z	x	y	z	S_{occ}
La	0.1984(3)	0.3462(8)	− 0.1775(5)	0.3486(2)	1/2	− 0.1792(5)	1
K	0.3511(9)	0.935(2)	0.686(1)	0.4274(5)	0	0.682(2)	1
O11	0.235(3)	0.187(2)	− 0.502(2)	0.369(1)	0.348(2)	− 0.510(2)	1
O21	0.245(3)	0.556(2)	− 0.504(1)				
O12	0.227(3)	0.180(2)	0.171(2)	0.355(1)	0.324(2)	0.162(2)	1
O22	0.213(3)	0.537(2)	0.165(1)				
O31	0.004(2)	0.234(1)	− 0.502(2)	0.248(1)	1/2	− 0.527(4)	1
O32	0.092(2)	− 0.012(1)	− 0.253(2)	0.303(2)	0.173(5)	− 0.263(3)	1/2
O41	0.411(1)	0.287(2)	− 0.147(3)	0.4510(5)	0.299(2)	− 0.074(3)	1
O42	0.3938(9)	0.625(2)	− 0.027(4)				
C1	0.242(3)	0.272(2)	− 0.664(2)	0.358(2)	0.4028(8)	− 0.683(1)	1
C2	0.215(3)	0.456(2)	− 0.671(1)				
C3	− 0.013(2)	0.072(1)	− 0.575(2)	0.239(1)	0.3362(9)	− 0.562(2)	1/2
C4	0.502(1)	0.401(2)	− 0.018(5)	1/2	0.3974(8)	0	1
Ow1	− 0.644(2)	− 0.052(4)	− 0.753(4)	− 0.065(1)	1/2	− 0.736(4)	1
Ow2	− 0.042(2)	0.200(4)	− 0.077(4)	0.221(1)	1/2	− 0.088(4)	1
Ow3	0.125(3)	0.647(3)	− 0.180(5)	0.303(2)	0.823(5)	− 0.147(6)	1/2

Note. $B_{overall}$: 1.28(7) Å^2 (triclinic symmetry), 1.1(1) Å^2 (monoclinic symmetry). O21 in the triclinic subcell leads to the equivalent position x, $1 - y$, z of O11 in the monoclinic cell. I.d. for O22, O42, and C2. Ow3 corresponds approximately to the equivalent position x, $1 - y$, z of O32 in the monoclinic cell. No C atom in the triclinic subcell generates the equivalent position x, $1 - y$, z of C3 in the monoclinic cell.

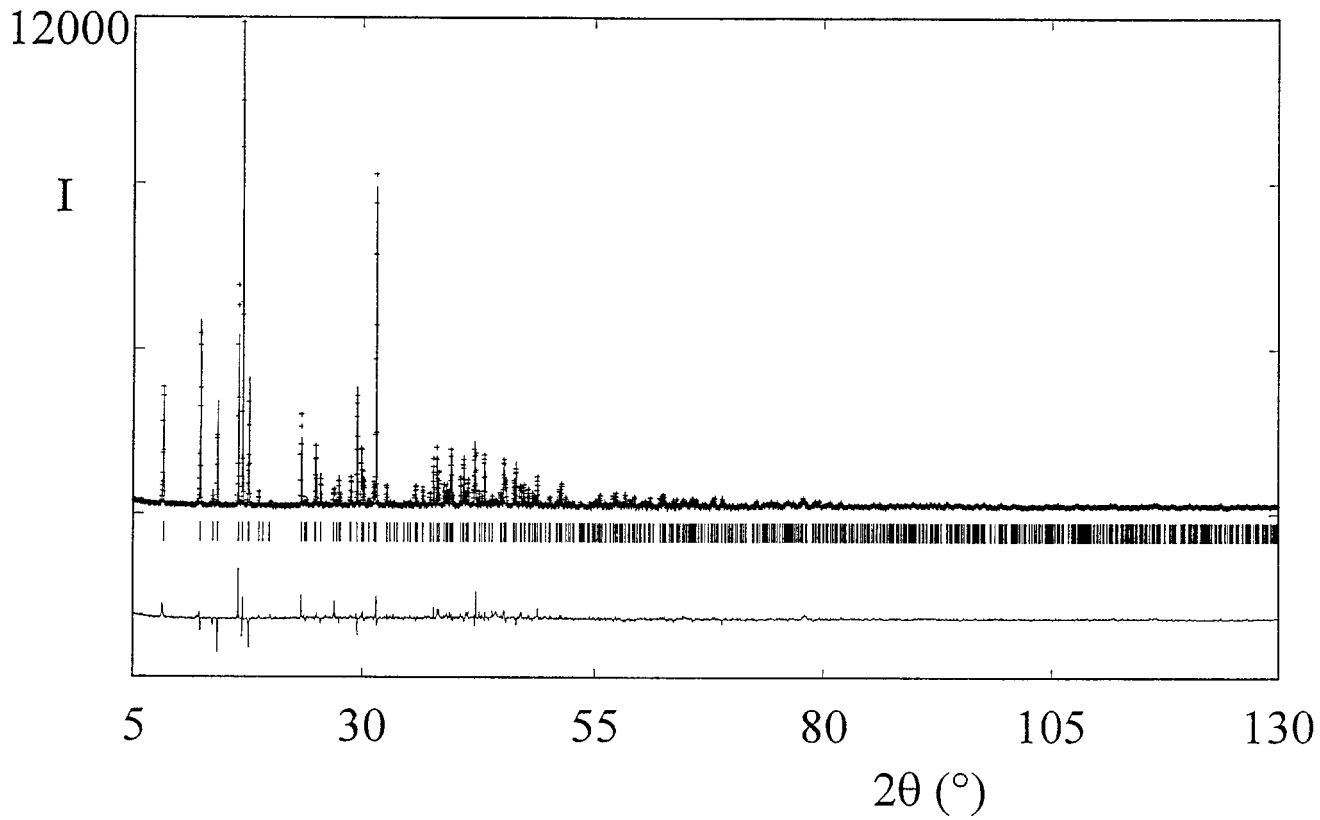

FIG. 3. Final Rietveld plot for $La(H_2O)_2K(C_2O_4)_2 \cdot H_2O$. The experimental data are represented by crosses, while the calculated pattern is shown by the solid line. The lower trace corresponds to the difference curve between observed and calculated patterns. The Bragg reflections are shown by the vertical bars.

TABLE 3
Bond Distances (Å) and Angles (°) for $La(H_2O)_2K(C_2O_4)_2 \cdot H_2O$ in the Triclinic Subcell

La polyhedron	La–O11	2.66(2)	La–O12	2.64(1)
	La–O21	2.74(1)	La–O22	2.64(1)
	La–O31	2.65(2)	La–O32	2.59(1)
	La–O41	2.63(2)	La–O42	2.55(1)
	La–Ow2	2.91(3)	La–Ow3	2.69(3)
K polyhedron	K–O11^{i}	2.83(2)	K–O21^{ii}	2.90(2)
	K–O41^{i}	2.70(2)	K–O42^{ii}	3.12(2)
	K–O32^{i}	3.28(3)	K–Ow3^{ii}	3.13(3)
	K–Ow1^{iii}	2.94(3)	K–Ow1^{iv}	3.16(3)
Ligand Ox1	C1–C2	1.53(3)	O11–C1–O12^{v}	118(2)
	C1–O11	1.26(2)	O11–C1–C2	118(2)
	C1–O12^{v}	1.25(2)	O12^{v}–C1–C2	120(2)
	C2–O21	1.26(1)	O21–C2–O22^{v}	117(1)
	C2–O22^{v}	1.25(1)	O21–C2–C1	118(2)
			O22^{v}–C2–C1	118(2)
Ligand Ox3	C3–C3^{vi}	1.54(2)	O31–C3–O32^{vi}	118(2)
	C3–O31	1.26(1)	O31–C3–C3^{vi}	118(1)
	C3–O32^{vi}	1.27(2)	O32^{vi}–C3–C3^{vi}	118(2)
Ligand Ox4	C4–C4^{vii}	1.54(2)	O41–C4–O42^{vii}	120(2)
	C4–O41	1.26(3)	O41–C4–C4^{vii}	118(2)
	C4–O42^{vii}	1.27(2)	O42^{vii}–C4–C4^{vii}	119(2)

Note. Symmetry operators: (i) $x, y+1, z+1$; (ii) $x, y, z+1$; (iii) $x+1, y+1, z+1$; (iv) $-x, -y+1, -z$; (v) $x, y, z-1$; (vi) $-x, -y, -z-1$; (vii) $-x+1, -y+1, -z$.

in the angular range 7–95° (2θ) containing 565 reflections, led to the residual factors $R_F = 0.082$ and $R_{wp} = 0.121$. Figure 4 shows the best agreement obtained between calculated and observed patterns for the triclinic subcell. Refined atomic coordinates in the triclinic and monoclinic cells are given in Table 4. Selected bonds and angles in the triclinic cell are listed in Table 5.

DESCRIPTION OF THE STRUCTURE OF $La(H_2O)_2K(C_2O_4)_2 \cdot H_2O$

Figure 5 shows the projection of the structure of $La(H_2O)_2K(C_2O_4)_2 \cdot H_2O$ on the plane (a, b). The structure consists of corrugated planes of lanthanum atoms linked by oxalate groups, parallel to (110). The potassium atoms and the water molecules Ow1 and Ow3 are intercalated between the layers. The bond La–Ow3 is perpendicular to the corrugated plane, and Ow3 coordinates the potassium atoms in the interlayer spacing. Figure 6 is a projection of the structure on the plane (a, c). It shows that the layers are formed by four-membered rings $[La(C_2O_4)]_4$. Ow2 lies on the plane in tunnels with diamond-shaped cross sections, while K and Ow1 are located in tunnels with an almost square cross section. The lanthanum atom is tenfold-coordinated to

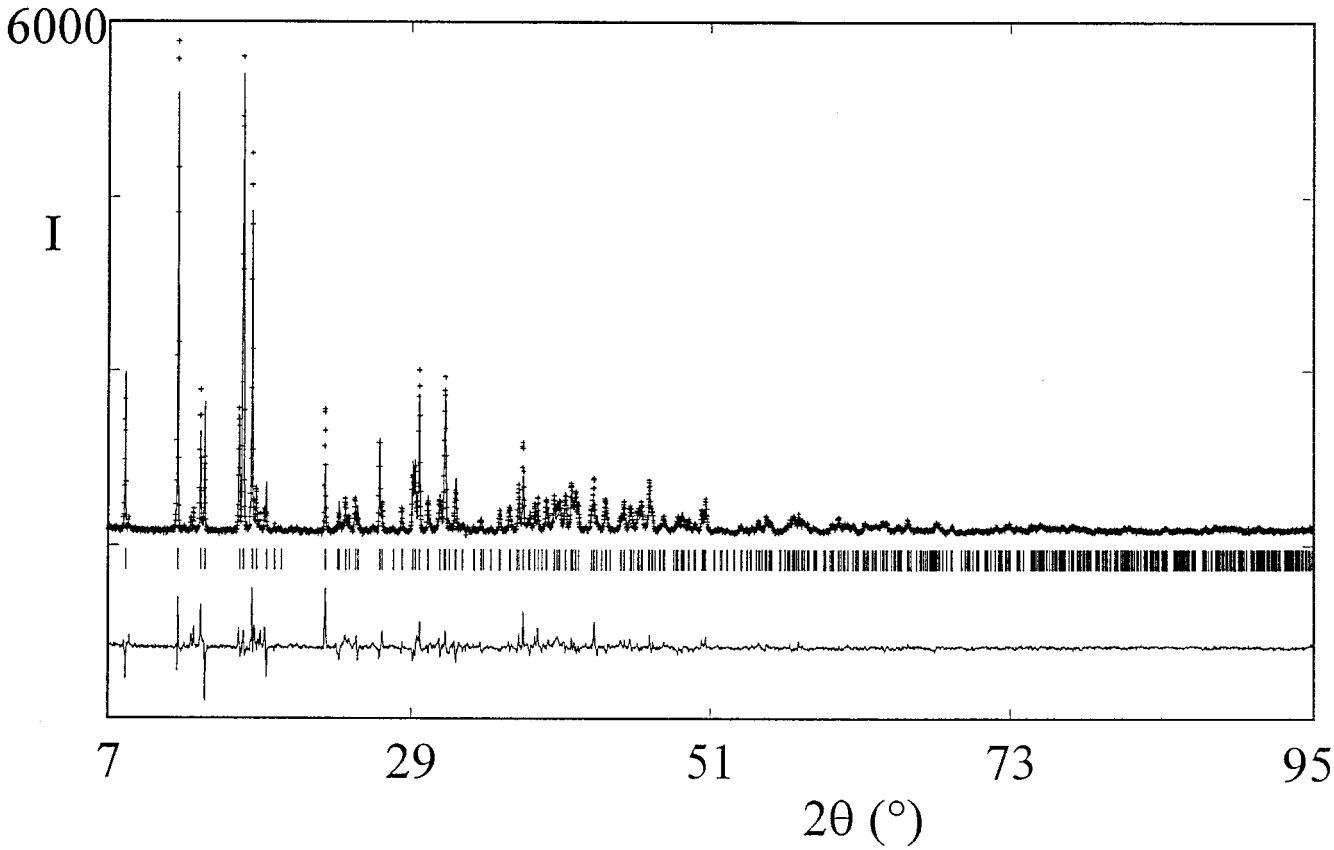

FIG. 4. Final Rietveld plot for $La(H_2O)_2(NH_4)(C_2O_4) \cdot H_2O$.

oxygen atoms in a distorted bicapped square antiprism, as seen in Fig. 7a. The coordination polyhedron is made of eight oxygen atoms of oxalate groups, which define the antiprism, and two bicapped water oxygen atoms, Ow2 and Ow3. The La-O distances fall into the range 2.55(1)-2.91(3) Å, which is in accordance with the bond distances calculated with the program VALENCE (24), i.e., 2.67 Å for tenfold-coordinated lanthanum atoms. The elongated bond is observed between Ow2 and La, while the La–Ow3 bond length [2.69(3) Å] is close to the mean distance, 2.64(1) Å, observed between La and oxygen atoms of the oxalate groups, since Ow3 and O32 are strongly correlated in the structure. The potassium atom is eightfold-coordinated to the oxygen atoms in a slightly distorted dodecahedron, as shown in Fig. 7b. The K–O distances vary in the wide range 2.70(2)–3.28(3) Å. The mean distance obtained from the program VALENCE for eightfold-coordinated potassium atoms is 2.90 Å, while the mean K–O distance observed here is 3.01(3) Å with five contacts greater than 2.90 Å. Moreover, the shortened bond lengths are observed between K and some oxygen atoms from the oxalate groups in the layers. Then, the K atom is likely to be weakly bonded to the water molecules in the interlayer spacing. All the oxalate groups are bidentate toward the lanthanum atom, while ligand Ox4 only is bidentate toward the potassium atom. The mean C–C distance is 1.54(2) Å and the mean C–O distance is 1.26(2) Å. The three independent water molecules have chemically different functions in the structure. Ow1 is connected only to two potassium atoms in the interlayer spacing. Ow2 coordinates only one lanthanum atom in the corrugated plane parallel to (110). Ow3 is located in the interlayer spacing and coordinates both the potassium and the lanthanum atoms.

It is of interest to study the environment of the water molecules in order to understand the role of hydrogen bonding in the structures of $La(H_2O)_2K(C_2O_4)_2 \cdot H_2O$ and $La(H_2O)_2(NH_4)(C_2O_4)_2 \cdot H_2O$. The investigation of possible hydrogen bonds was based on the criteria defined by Baur and Khan (25) and, later, by Baur (26), which are related to contacts between water molecules and adjacent oxygen atoms. The conditions given by these authors were extended to contacts between N and acceptor oxygens in the structure of $La(H_2O)_2(NH_4)(C_2O_4)_2 \cdot H_2O$. Upon the selected contacts, there was an ambiguous hydrogen bonding scheme between Ow2 and Ow3 in the structure of $La(H_2O)_2K(C_2O_4)_2 \cdot H_2O$, since it was not possible to determine whether Ow3 is a donor atom or an acceptor atom. Then, it was decided to confer a tetrahedral environment for

TABLE 4
Fractional Atomic Coordinates for $La(H_2O)_2(NH_4)(C_2O_4)_2 \cdot H_2O$ in the Triclinic Subcell (S.G. $P\bar{1}$) and the Monoclinic Cell (S.G. $C2/m$) (S_{occ}: site occupancy factor)

	$P\bar{1}$			$C2/m$				
	x	y	z		x	y	z	S_{occ}
La	0.1951(5)	0.349(2)	− 0.1534(7)	La	0.3469(2)	1/2	− 0.1535(6)	1
N	0.398(4)	0.97(1)	0.656(7)	N	0.455(2)	0	0.650(6)	1
O11	0.214(4)	0.186(2)	− 0.486(2)	O11	0.3511(9)	0.373(2)	− 0.524(2)	1
O21	0.294(4)	0.563(2)	− 0.447(2)					
O12	0.189(4)	0.188(2)	0.179(2)	O12	0.3470(9)	0.315(2)	0.165(2)	1
O22	0.251(4)	0.562(2)	0.216(2)					
O31	− 0.068(3)	0.159(4)	− 0.442(3)	O31	0.231(2)	1/2	− 0.505(2)	1
O32	0.068(4)	− 0.048(6)	− 0.246(2)	O32	0.304(2)	0.182(4)	− 0.250(6)	1/2
O41	0.407(1)	0.277(2)	− 0.106(6)	O41	0.4470(5)	0.334(2)	− 0.052(3)	1
O42	0.391(1)	0.612(3)	− 0.020(6)					
C1	0.209(6)	0.270(2)	− 0.647(2)	C1	0.3720(8)	0.4015(9)	− 0.681(1)	1
C2	0.268(5)	0.480(2)	− 0.627(2)					
C3	− 0.052(4)	0.042(6)	− 0.553(2)	C3	0.205(3)	0.3106(9)	− 0.573(2)	1/2
C4	0.505(2)	0.411(3)	− 0.04(1)	C4	1/2	0.4015(8)	0	1
Ow1	− 0.629(4)	− 0.08(1)	− 0.745(5)	Ow1	− 0.070(1)	1/2	− 0.699(4)	1
Ow2	− 0.026(4)	0.20(1)	− 0.060(5)	Ow2	0.245(2)	1/2	− 0.014(4)	1
Ow3	0.152(4)	0.668(6)	− 0.140(6)	Ow3	0.330(2)	0.789(5)	− 0.143(4)	1/2

Note. $B_{overall}$: 0.1(2) Å^2 (triclinic symmetry), 1.1(1) Å^2 (monoclinic symmetry).

water oxygen atoms. The following condition was thus added to the criteria given by Baur and Khan (25) and by Baur (26): a water oxygen atom cannot be linked to more than two cations (including H atoms) through its lone-pair orbitals. This is in agreement with the largest number of hydrates encountered in the literature, although some were found to have fivefold-coordinated water oxygen atoms (27). With this additional criterion, Ow3 is obviously a donor oxygen, since it is already linked to La and K. The three water oxygen atoms are then tetrahedrally surrounded in the two structures. Table 6 displays the possible hydrogen bonds for $La(H_2O)_2K(C_2O_4)_2 \cdot H_2O$ and $La(H_2O)_2(NH_4)(C_2O_4)_2 \cdot H_2O$, which includes hydrogen bonding from the NH_4 group.

It is worth noting that a similar layered-type structure was recently described for $Y(H_2O)Na(C_2O_4)_2 \cdot 3H_2O$, in which Na atoms and water molecules are also intercalated between $[Y(C_2O_4)^-]_\infty$ planes (10). The widest review of the structures of mixed oxalates, including rare earth or yttrium elements and monovalent cations, showed that the structure of $YNH_4(C_2O_4)_2 \cdot H_2O$ (28) is also related to this type, though the authors did not report this feature. A schematic view of the layered structures of the related yttrium ammonium and yttrium sodium oxalates is given in Fig. 8.

TABLE 5
Bond Distances (Å) and Angles (°) for $La(H_2O)_2(NH_4)(C_2O_4)_2 \cdot H_2O$ in the Triclinic Subcell

La polyhedron	La–O11	2.64(3)	La–O12	2.55(2)
	La–O21	2.79(2)	La–O22	2.77(2)
	La–O31	3.07(3)	La–O32	2.94(4)
	La–O41	2.67(2)	La–O42	2.47(2)
	La–Ow2	2.69(6)	La–Ow3	2.70(5)
Ligand Ox1	C1–C2	1.54(2)	O11–C1–O12^i	121(2)
	C1–O11	1.25(2)	O11–C1–C2	119(2)
	C1–O12^i	1.26(3)	O12^i–C1–C2	117(2)
	C2–O21	1.28(2)	O21–C2–O22^i	120(2)
	C2–O22^i	1.24(2)	O21–C2–C1	117(2)
			O22^i–C2–C1	119(2)
Ligand Ox3	C3–C3^{ii}	1.58(6)	O31–C3–O32^{ii}	122(3)
	C3–O31	1.27(5)	O31–C3–C3^{ii}	117(5)
	C3–O32^{ii}	1.31(2)	O32^{ii}–C3–C3^{ii}	114(4)
Ligand Ox4	C4–C4^{iii}	1.53(5)	O41–C4–O42^{iii}	120(4)
	C4–O41	1.25(4)	O41–C4–C4^{iii}	119(4)
	C4–O42^{iii}	1.25(4)	O42^{iii}–C4–C4^{iii}	118(3)

Note. Symmetry operators: (i) $x, y, z - 1$; (ii) $-x, -y, -z - 1$; (iii) $-x + 1, -y + 1, -z$.

THERMAL DECOMPOSITION OF $La(H_2O)_2M(C_2O_4)_2 \cdot H_2O$ (M = K, NH_4)

1. *Thermal Decomposition of $La(H_2O)_2K(C_2O_4)_2 \cdot H_2O$*

Dehydration of the precursor. The TG curve (Fig. 9) shows that the dehydration starts at $\sim 36°C$ and proceeds through three successive stages. A loss of 0.5 H_2O is observed during the first stage between 36 and 64°C (observed

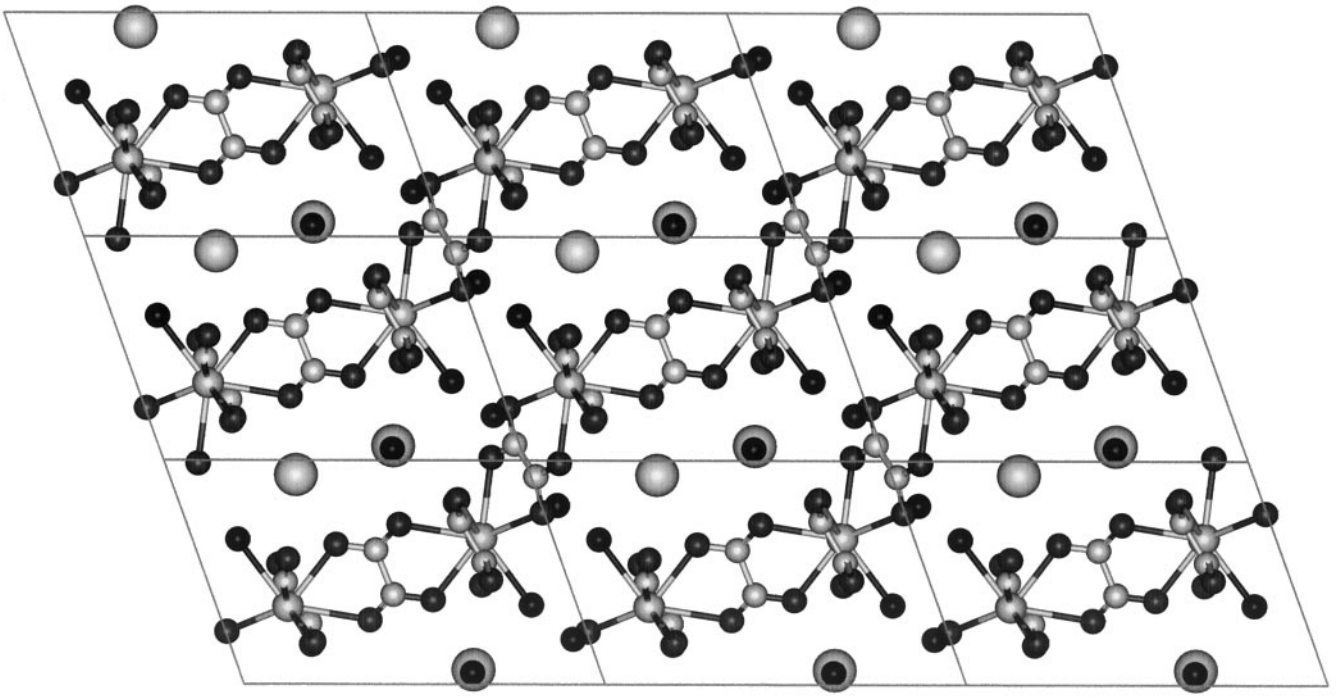

FIG. 5. Projection of the structure along the c axis (a horizontal) of $La(H_2O)_2K(C_2O_4)_2 \cdot H_2O$, showing the potassium atoms and the water molecules between the layers. Large gray circles, K; small gray circles, C; small dark circle, O.

weight loss at the inflection: 2.2%). The second stage is characterized by the departure of 2.27 water molecules from 64 to 100°C (total weight loss at 100°C: 12.2%). The remaining water molecules are released continuously in the third stage in the wide temperature range 100–220°C to form the anhydrous phase $LaK(C_2O_4)_2$. From the total weight loss (13.8%) observed at 220°C, it can be stated that the amount of water molecules in the precursor is 3.13 at room temperature. These stages are summarized in Table 7.

The TDXD plot (Fig. 10) of the successive powder diffraction patterns, collected during the thermal decomposition of $La(H_2O)_2K(C_2O_4)_2 \cdot H_2O$, shows that the dehydration process does not involve any modification of the patterns until 100°C, where the content of the water molecule is only 0.36

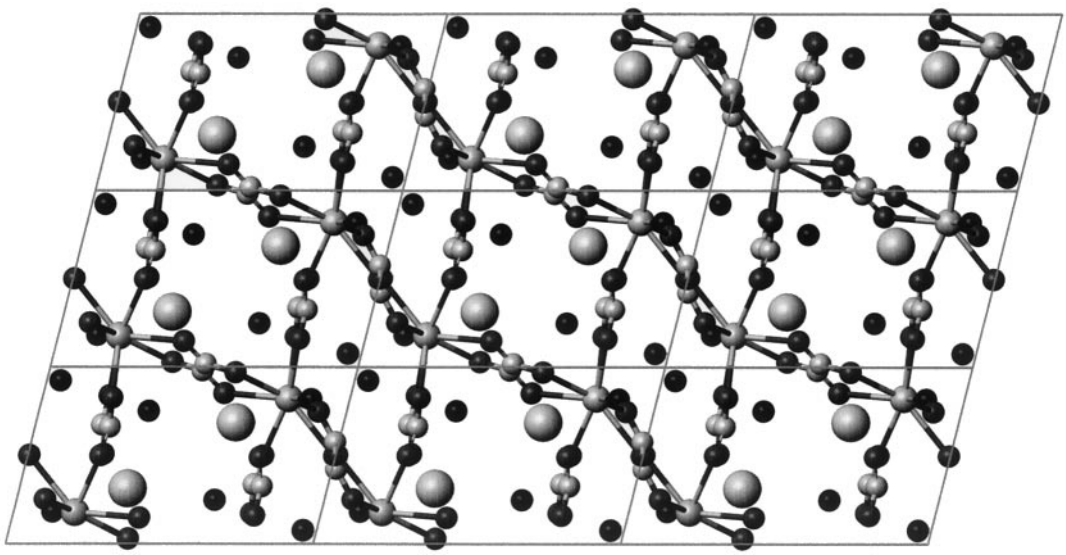

FIG. 6. Projection of the structure along the b axis (a horizontal) of $La(H_2O)_2K(C_2O_4)_2 \cdot H_2O$, showing the four-membered rings $[La(C_2O_4)]_4$.

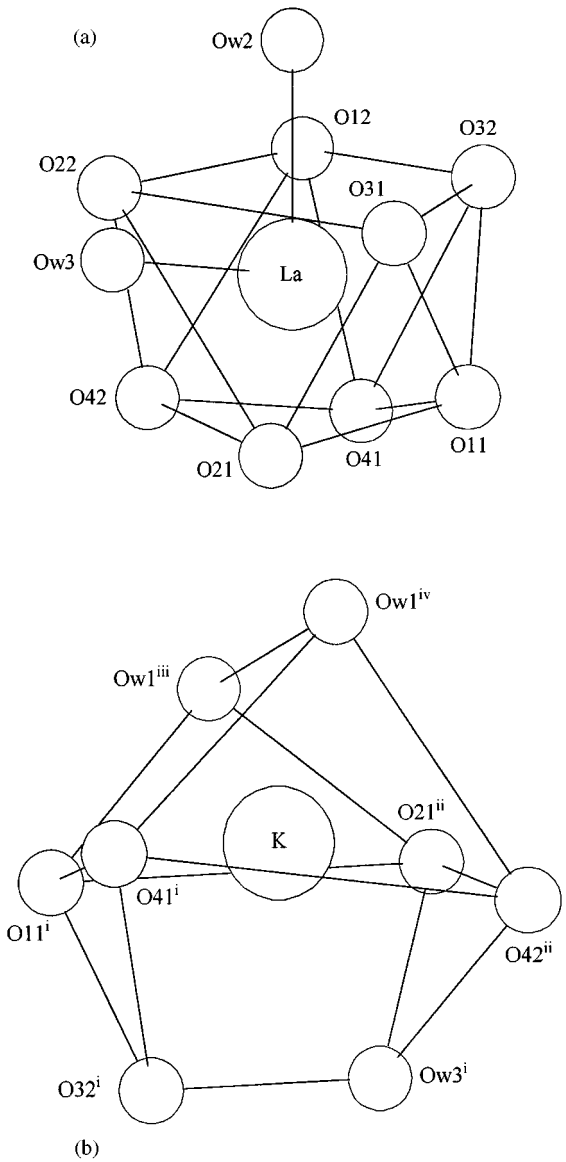

FIG. 7. Environments of (a) the La atom in a distorted bicapped square antiprism and (b) the K atom in a distorted dodecahedron.

per chemical formula. This feature demonstrates that the removal of the water molecules and the structure change are not simultaneous. Above 100°C the solid becomes rapidly amorphous to X-rays.

Crystallization of $LaK(C_2O_4)_2$. Figure 10 shows that the diffraction lines of a phase emerge from the background from 270°C, and their intensity increases up to 300°C. The formation of this phase seems to be accompanied by a weight loss of only 1.5% in this temperature range, as depicted by the TG curve (Fig. 9). To determine the nature of this phase, three successive diffraction patterns were recorded at 260°C from the amorphous solid obtained after the total dehydration of the precursor under flowing nitrogen (Fig. 11). The first pattern clearly shows that a crystallization process occurs during data collection over ~ 8 h. The second pattern points out the formation of a crystalline phase. To confirm this crystallization process, a TG-DSC run was performed at a heating rate of 60°C h^{-1} in nitrogen (Fig. 12). The DSC curve clearly displays an exothermic peak between 290 and 320°C while the weight loss indicated by the TG curve is very small ($< 1\%$). It is obvious that this thermal effect is associated with the crystallization phenomenon depicted by the TDXD plot (Fig. 10), though the temperature ranges over which these events are observed are slightly different, due to different heating rates. From these results it can be stated that the amorphous phase $LaK(C_2O_4)_2$ crystallizes. In spite of the modest quality of the second diffraction pattern in Fig. 11, the indexing based on the first 20 diffraction lines (except the spurious line situated at 29.45° (2θ) discussed afterward) was successful and gave a monoclinic solution with the cell parameters $a = 5.687(3)$ Å, $b = 15.241(5)$ Å, $c = 9.017(4)$ Å, $\beta = 92.82(3)°$, $V = 780.6(4)$ Å^3, with the likely space group $P2_1/c$

TABLE 6
Distances (Å) and Angles (°) for Possible Hydrogen Bonds for $La(H_2O)_2K(C_2O_4)_2 \cdot H_2O$ and $La(H_2O)_2(NH_4)(C_2O_4)_2 \cdot H_2O$ in the Triclinic Subcell

$La(H_2O)_2K(C_2O_4)_2 \cdot H_2O$		$La(H_2O)_2(NH_4)(C_2O_4)_2 \cdot H_2O$	
$Ow1 \cdots O12^{i}$	2.65(4)	$N \cdots Ow1^{vii}$	2.63(6)
$Ow1 \cdots O22^{ii}$	3.00(3)	$N \cdots Ow1^{v}$	2.46(8)
$Ow2 \cdots O12^{iii}$	2.94(3)	$N \cdots O21^{viii}$	3.01(9)
$Ow3 \cdots O31^{iv}$	2.64(3)	$N \cdots O41^{ix}$	2.81(8)
$Ow3 \cdots Ow2^{v}$	2.56(4)	$Ow1 \cdots O22^{ii}$	2.64(8)
		$Ow2 \cdots O12^{iii}$	2.98(8)
K^{ii}–Ow1–K^{v}	96.8(9)	$Ow3 \cdots O31^{iv}$	3.17(5)
K^{ii}–$Ow1 \cdots O12^{i}$	94(1)	$Ow3 \cdots Ow2^{v}$	2.64(7)
K^{v}–$Ow1 \cdots O12^{i}$	125(1)		
K^{ii}–$Ow1 \cdots O22^{ii}$	91.4(9)	$Ow1^{vii} \cdots N \cdots Ow1^{v}$	94(3)
K^{v}–$Ow1 \cdots O22^{ii}$	116(1)	$Ow1^{vii} \cdots N \cdots O21^{viii}$	74(3)
$O12^{i} \cdots Ow1 \cdots O22^{ii}$	117(1)	$Ow1^{v} \cdots N \cdots O21^{viii}$	110(4)
		$Ow1^{vii} \cdots N \cdots O41^{ix}$	130(3)
La–$Ow2 \cdots Ow3$	127(2)	$Ow1^{v} \cdots N \cdots O41^{ix}$	90(3)
La–$Ow2 \cdots O12^{iii}$	128(1)	$O21^{viii} \cdots N \cdots O41^{ix}$	148(3)
$Ow3^{v} \cdots Ow2 \cdots O12^{iii}$	104(1)		
		$N^{ii} \cdots Ow1 \cdots N^{v}$	86(3)
La–Ow3–K^{vi}	98.5(9)	$N^{ii} \cdots Ow1 \cdots O22^{ii}$	97(3)
La–$Ow3 \cdots O31^{iv}$	128(1)	$N^{v} \cdots Ow1 \cdots O22^{ii}$	118(4)
K^{vi}–$Ow3 \cdots O31^{iv}$	82(1)		
La–$Ow3 \cdots Ow2^{v}$	134(2)	La–$Ow2 \cdots Ow3^{v}$	134(3)
K^{vi}–$Ow3 \cdots Ow2^{v}$	112(1)	La–$Ow2 \cdots O12^{iii}$	123(2)
$O31^{iv} \cdots Ow3 \cdots Ow2^{v}$	92(1)	$Ow3^{v} \cdots Ow2 \cdots O12^{iii}$	103(3)
		La–$Ow3 \cdots Ow2^{v}$	134(3)
		La–$Ow3 \cdots O31^{iv}$	120(2)
		$Ow2^{v} \cdots Ow3 \cdots O31^{iv}$	94(2)

Note. Symmetry operators: (i) $x-1, y, z-1$; (ii) $x-1, y-1, z-1$; (iii) $-x, -y, -z$; (iv) $-x, -y+1, -z-1$; (v) $-x, -y+1, -z$; (vi) $x, y, z-1$; (vii) $x+1, y+1, z+1$; (viii) $x, y, z+1$; (ix) $x, y+1, z+1$.

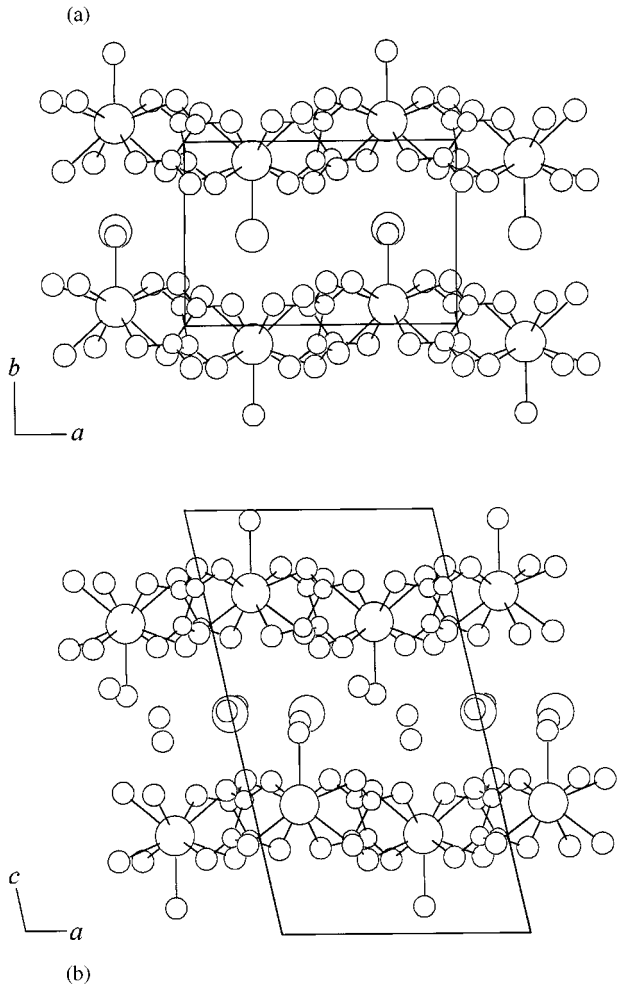

FIG. 8. Projection of the layered-type structure of (a) $YNH_4(C_2O_4)_2 \cdot H_2O$ along c (28) and (b) $Y(H_2O)Na(C_2O_4)_2 \cdot 3H_2O$ along b (10)

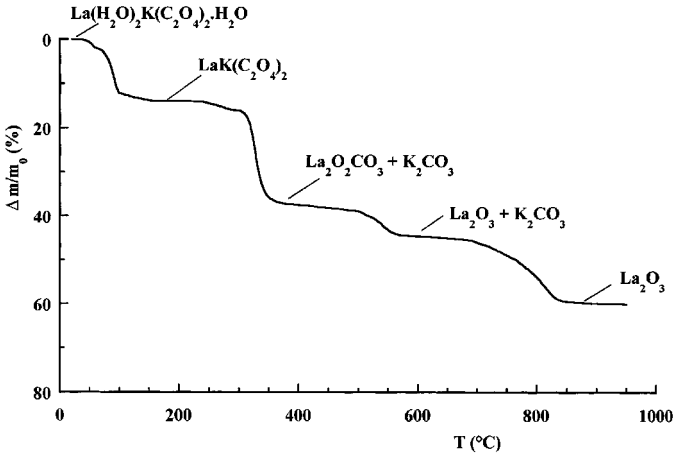

FIG. 9. TG curve for the decomposition of $La(H_2O)_2K(C_2O_4)_2 \cdot H_2O$ under flowing nitrogen (10°C h^{-1} from 20 to 180°C, 4°C h^{-1} from 180 to 950°C).

[$M_{20} = 32$, $F_{20} = 51(0.009,43)$]. The powder data have been submitted to the ICDD (22) for possible inclusion in the Powder Diffraction File. To our knowledge, this is the first time that an anhydrous rare earth oxalate has been obtained in a crystalline state and characterized. Indeed, the few anhydrous rare earth oxalates reported in the literature (29, 30) are known to be unstable and in an amorphous state.

From Fig. 11, it can be seen that the intensity of the line situated at 29.45° (2θ) slightly increases as a function of time as revealed by the third diffraction pattern recorded after 62 h. This is the strongest line of the diffraction pattern of the monoclinic variety $La_2O_2CO_3$ (Type-Ia) (31), which is one of the decomposition products of $LaK(C_2O_4)_2$ as described below. Consequently, it can be concluded that the crystallization of $LaK(C_2O_4)_2$ and the beginning of its decomposition take place simultaneously. This conclusion is supported by the TG curves in Figs. 9 and 12, which show that a slight weight loss is observed during the crystallization process. This feature was confirmed by a complementary TG experiment (precursor heated at 50°C h^{-1} from ambient temperature to 260°C and maintained at 260°C for 110 h) which displayed a total weight loss of 20% at the end of the run.

TABLE 7
Successive Stages of the Thermal Decomposition of $La(H_2O)_2K(C_2O_4)_2 \cdot H_2O$ under Flowing Nitrogen

Stage	Transformation	$\Delta m/m_0$ (%) observed	$\Delta m/m_0$ (%) calculated	Temperature range (°C) TG/TDXD
1	$LaK(C_2O_4)_2 \cdot 3.13H_2O \rightarrow LaK(C_2O_4)_2 \cdot 2.63H_2O + 0.5H_2O^{\uparrow}$	2.2	—	36–64
2	$LaK(C_2O_4)_2 \cdot 2.63H_2O \rightarrow LaK(C_2O_4)_2 \cdot 0.36H_2O + 2.27H_2O^{\uparrow}$	12.2	—	64–100
3	$LaK(C_2O_4)_2 \cdot 0.36H_2O \rightarrow LaK(C_2O_4)_{2(am)} + 0.36H_2O^{\uparrow}$	13.8	—	100–220
4	$LaK(C_2O_4)_{2(am)} \rightarrow LaK(C_2O_4)_{2(cr)}$	—	—	270–300
5	$LaK(C_2O_4)_{2(cr)} \rightarrow 1/2La_2O_2CO_3$ (Type-Ia) $+ 1/2K_2CO_3 + CO_2^{\uparrow} + 2CO^{\uparrow}$	37	38.1	315–370
6	$1/2La_2O_2CO_3$ (Type-Ia) $\rightarrow 1/2La_2O_2CO_3$ (Type-II)	—	—	420
7	$1/2La_2O_2CO_3$ (Type-II) $\rightarrow 1/2La_2O_3 + 1/2CO_2^{\uparrow}$	44	43.5	510–580
8	$1/2K_2CO_3 \rightarrow 1/2K_2O^{\uparrow} + 1/2CO_2^{\uparrow}$	60	60.3	690–835

Note. Here, (am) and (cr) denote amorphous and crystalline phases, respectively.

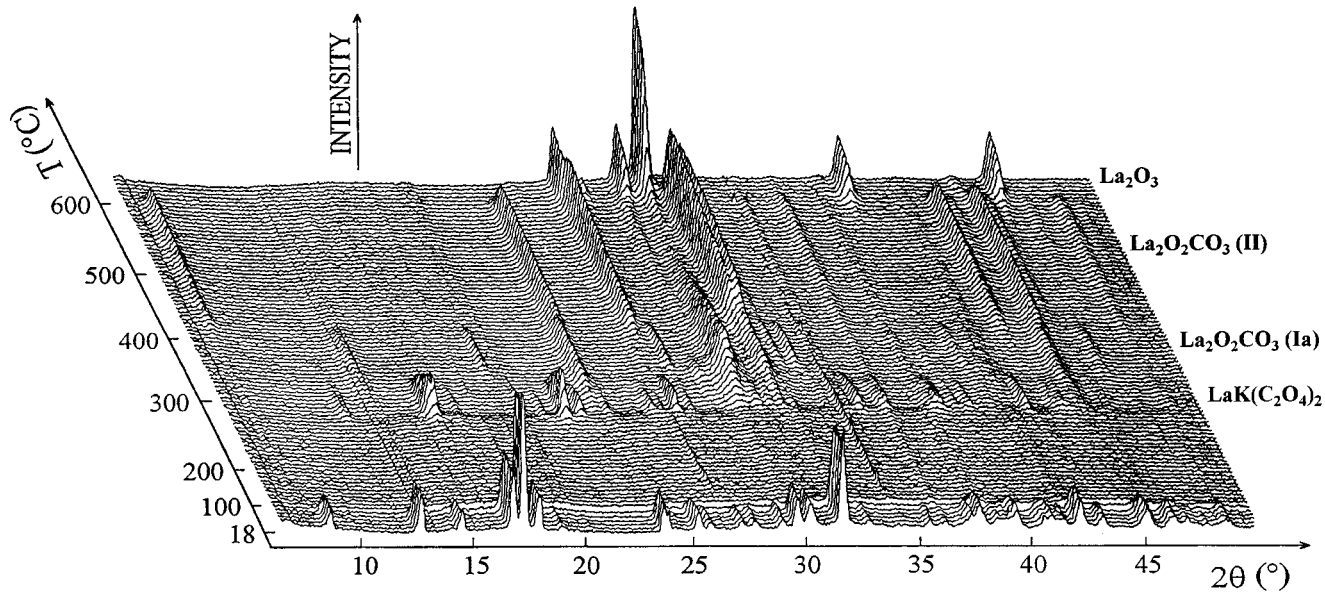

FIG. 10. TDXD plot for $La(H_2O)_2K(C_2O_4)_2 \cdot H_2O$ under flowing nitrogen ($10°C\,h^{-1}$ from 20 to 180°C, $4°C\,h^{-1}$ from 180 to 620°C, counting time of 5400 s per pattern).

Decomposition of $LaK(C_2O_4)_2$. The TG curve (Fig. 9) shows that $LaK(C_2O_4)_2$ loses weight rapidly between 315 and 370°C. From 370 to 510°C, the rate of the weight loss slows down since the weight loss is only 2% in this temperature range. At 370°C, the total weight loss achieves 37%, in agreement with the formation of a solid with the global

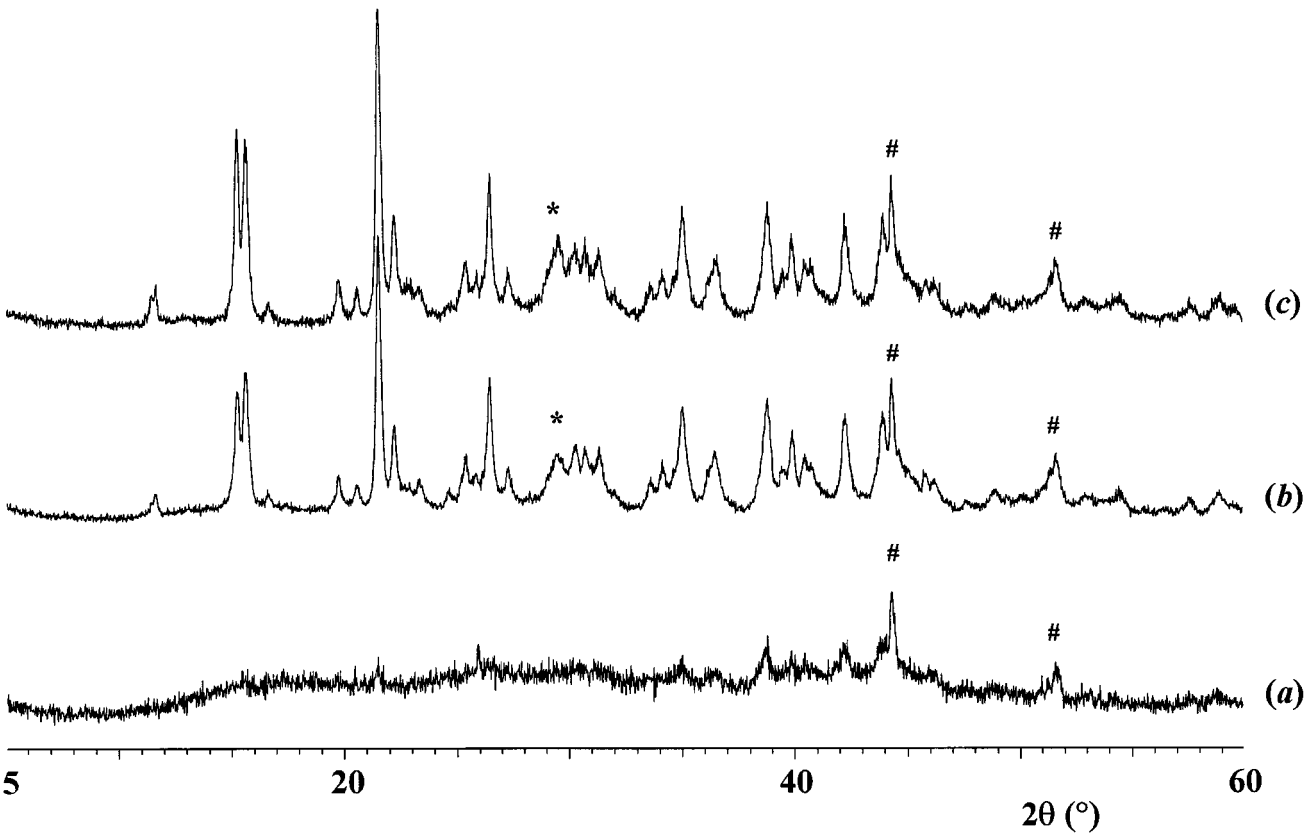

FIG. 11. Powder X-ray diffraction patterns of $LaK(C_2O_4)_2$ at 260°C [step length 0.02° (2θ), time $step^{-1}$ (a) 17 s, (b) 65 s, (c) 33 s]. The asterisks correspond to the strongest diffraction line of $La_2O_2CO_3$. The pound signs indicate diffraction lines of the sample holder (Ni).

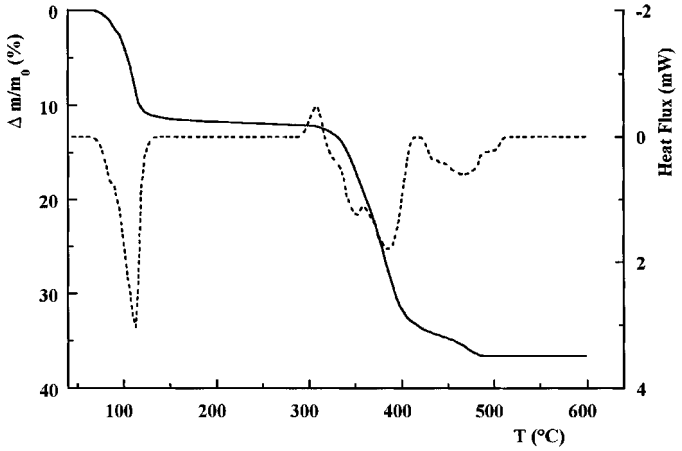

FIG. 12. TG-DSC curves for the decomposition of $La(H_2O)_2K(C_2O_4)_2 \cdot H_2O$ under flowing nitrogen (60°C h^{-1} from 40 to 600°C, sample mass 17.31 mg).

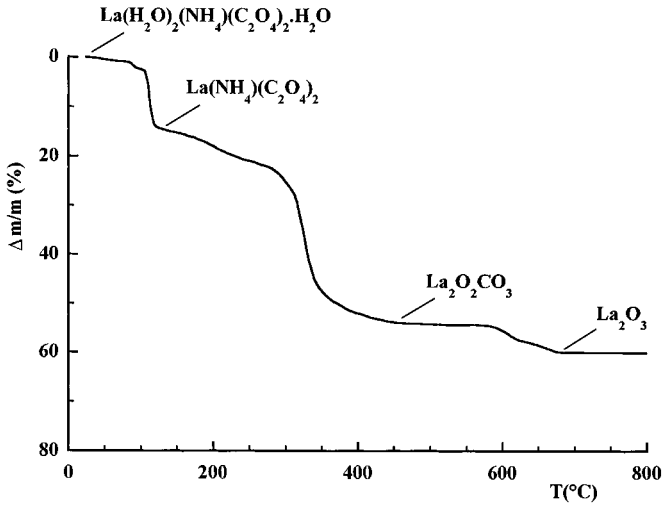

FIG. 13. TG curve for the decomposition of $La(H_2O)_2(NH_4)(C_2O_4)_2 \cdot H_2O$ under flowing air (5°C h^{-1} from 20 to 450°C, 20°C h^{-1} from 450 to 800°C).

composition "$LaKOCO_3$" (theoretical weight loss 38.1%). Furthermore, the TDXD plot displays only the diffraction lines of monoclinic $La_2O_2CO_3$ (Type-Ia). Consequently the simultaneous formation of amorphous K_2CO_3 must be put forward in order to balance the mass. Then, $La_2O_2CO_3$ (Type-Ia) transforms at 420°C into the hexagonal form (Type-II) (32) as described by Sawyer *et al.* (31) and, recently, by Gobichon *et al.* (33). However, it can be noted that it is the first time that this transformation has been observed at such a low temperature. Moreover, it is worthwhile pointing out that the decomposition of $LaK(C_2O_4)_2$ yields directly monoclinic $La_2O_2CO_3$ (Type-Ia), followed by hexagonal $La_2O_2CO_3$ (Type-II), while that of lanthanum oxalate gives the usual sequence Type-I → Type-Ia → Type-II (31, 34, 35). The direct formation of $La_2O_2CO_3$ (Type-Ia) is also observed when the decomposition is carried out under flowing air or under vacuum.

As depicted by the TG curve (Fig. 9), the rate of the weight loss is low from ~ 420 to 510°C and fast between 510 and 580°C. The TDXD plot (Fig. 10) clearly shows the vanishing of the lines of $La_2O_2CO_3$ (Type-II) and the appearance of those of hexagonal La_2O_3. Consequently, it can be concluded that $La_2O_2CO_3$ decomposes into La_2O_3, in agreement with the weight loss of 44% obtained at 580°C (theoretical 43.5%), while K_2CO_3 remains stable and amorphous. In the last stage, the total decomposition of K_2CO_3 occurs from ~ 580°C to ~ 835°C (final weight loss 60%). Surprisingly, amorphous K_2CO_3 is remarkably unstable, since it is known that pure potassium carbonate decomposes only above its melting point (891°C). A similar feature was recently reported during the decomposition of $YK(C_2O_4)_2 \cdot 4H_2O$ (7).

The successive stages of the decomposition of $LaK(C_2O_4)_2$ are summarized in Table 7 (stages 5 to 8).

2. *Thermal Decomposition of $La(H_2O)_2(NH_4)(C_2O_4)_2 \cdot H_2O$*

The successive stages of the thermal decomposition of $La(H_2O)_2(NH_4)(C_2O_4)_2 \cdot H_2O$, carried out under flowing air, are summarized in Table 8, as deduced from the TG curve (Fig. 13) and the TDXD plot (Fig. 14). Some differences with regard to the decomposition scheme of $La(H_2O)_2K(C_2O_4)_2 \cdot H_2O$ worthy of comment follow:

(i) The dehydration of the precursor leads directly to poorly crystalline $La(NH_4)(C_2O_4)_2$. Its diffraction pattern is

TABLE 8
Successive Stages of the Thermal Decomposition of $La(H_2O)_2(NH_4)(C_2O_4)_2 \cdot H_2O$ under Flowing Air

Stage	Transformation	$\Delta m/m_0$ (%) observed	$\Delta m/m_0$ (%) calculated	Temperature range (°C) TG
1	$La(NH_4)(C_2O_4)_2 \cdot 3H_2O \rightarrow La(NH_4)(C_2O_4)_2 \cdot 2.5H_2O + 0.5H_2O^{\uparrow}$	2.3	—	20–100
2	$La(NH_4)(C_2O_4)_2 \cdot 2.5H_2O \rightarrow La(NH_4)(C_2O_4)_2 + 2.5H_2O^{\uparrow}$	14.0	—	100–122
3	$La(NH_4)(C_2O_4)_2 \rightarrow 1/2La_2O_2CO_3$ (Type-II) $+ NH_3^{\uparrow} + 1/2H_2^{\uparrow} + 2CO_2^{\uparrow} + 3/2CO^{\uparrow}$	52.2	52.2	122-410
4	$1/2La_2O_2CO_3$ (Type-II) $\rightarrow 1/2La_2O_3 + 1/2CO_2^{\uparrow}$	59	57.9	410–680

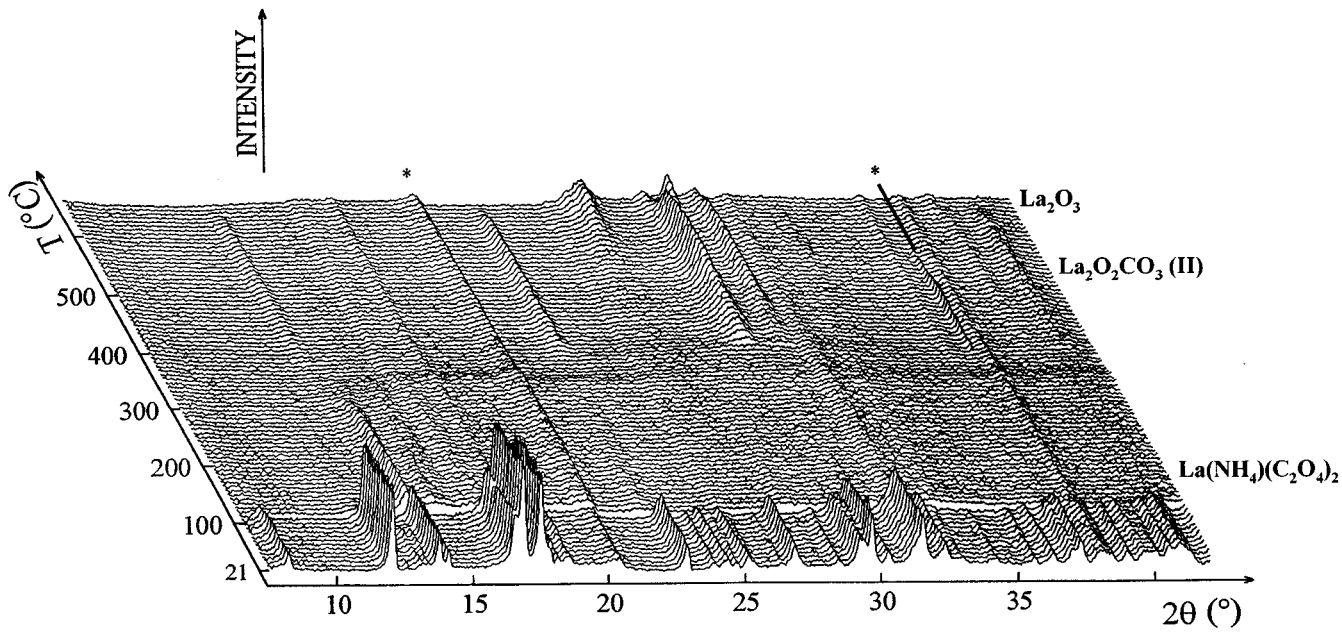

FIG. 14. TDXD plot for $La(H_2O)_2(NH_4)(C_2O_4)_2 \cdot H_2O$ under flowing air ($5°C\,h^{-1}$ from 20 to 620°C, counting time of 5400 s per pattern). The asterisks indicate spurious lines from the sample holder.

given in Fig. 15. Although the positions of the broad lines are not precisely defined, it is clear that $La(NH_4)(C_2O_4)_2$ is not isostructural with the related potassium compound.

(ii) $La(NH_4)(C_2O_4)_2$ is not stable. It decomposes from about 122°C and yields an amorphous solid beyond 300°C.

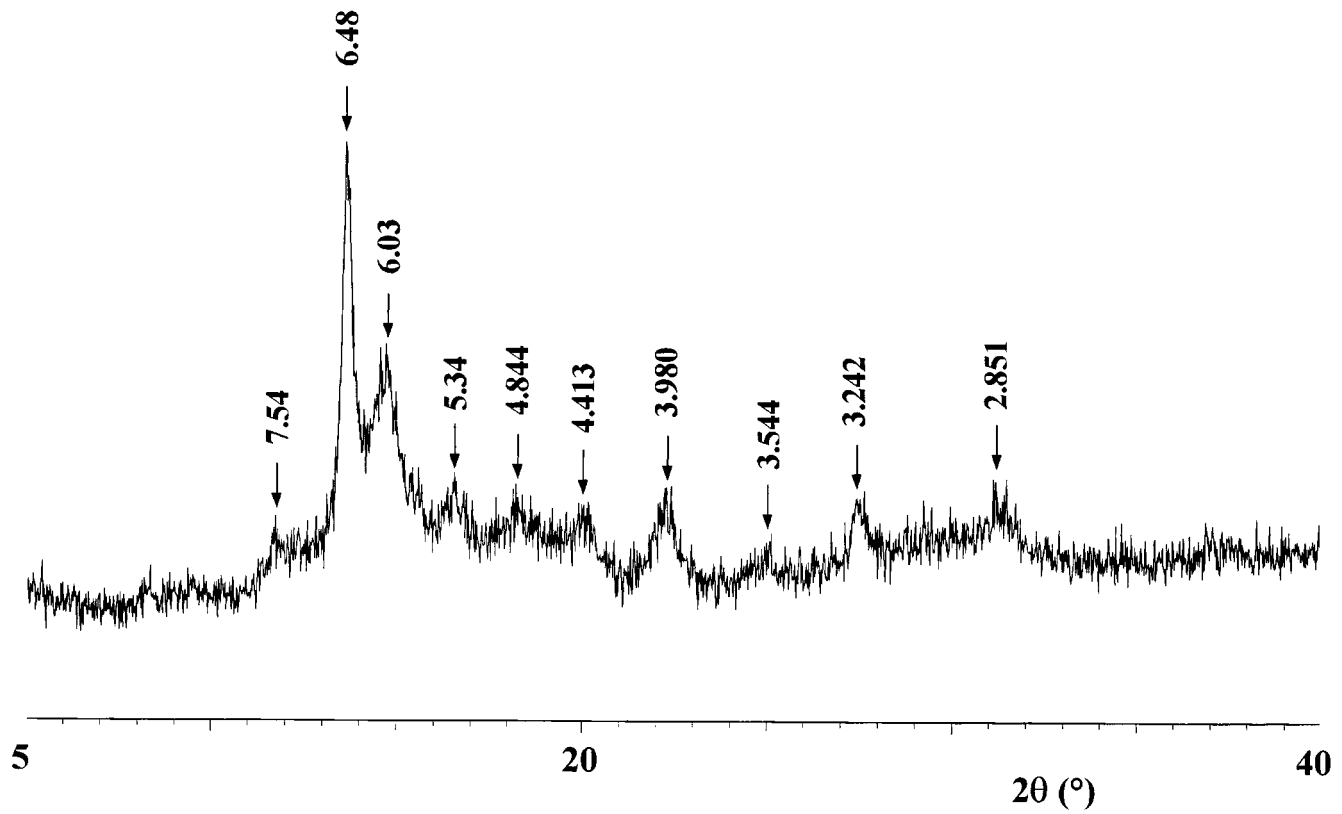

FIG. 15. Powder X-ray diffraction pattern of $La(NH_4)(C_2O_4)_2$ at 120°C (step length 0.02° 2θ, time $step^{-1}$ 20 s); *d*-spacings (Å) are indicated for the strongest diffraction lines.

(iii) At 410°C the anhydrous phase is completely decomposed into hexagonal $La_2O_2CO_3$ (Type-II), instead of the monoclinic variety (Type-Ia) reported from the decomposition of $LaK(C_2O_4)_2$.

CONCLUDING REMARKS

Despite the actual disorder in the crystal structure of $La(H_2O)_2M(C_2O_4)_2 \cdot H_2O$ (M = K, NH_4) in the monoclinic cell, from which arises a certain ambiguity regarding the position of half an oxalate group, the structure has been satisfactorily described in the triclinic subcell from the powder diffraction data collected with conventional laboratory X-rays. Except for the disorder problem, the structure reported in this study is likely basically correct and at least informative enough to allow a sensible chemical discussion of the structure properties. Indeed, the existence of layered structures is confirmed in the family and is also supported by the preferred orientation direction of the crystallites perpendicular to the layers. The layered nature of the structure of the ammonium compound sheds light on the noteworthy cation-exchange capabilities of the ammonium phase with regard to U(IV) and Th. Indeed, Stella *et al.* (11) claimed to obtain U(IV)-saturated, as well as Th-saturated (12, 13), lanthanum ammonium oxalates with the chemical formula $La_6M^{IV}(NH_4)_2(C_2O_4)_{12} \cdot 6H_2O$ (M = U, Th). A relevant explanation of this feature is the exchange of two-thirds of both the ammonium cations and the water molecules, located in the interlayer spacing of the structure of $La(H_2O)_2(NH_4)(C_2O_4)_2 \cdot H_2O$, by the transuranium cations. From the layered-type structures of the compounds of this oxalate family, namely, the isostructural lanthanum potassium oxalate, yttrium sodium oxalate (10), and yttrium ammonium oxalate (28), it can be suggested that similar ion-exchange properties could also be expected. Finally, the study of the thermal decomposition of the two phases, carried out with temperature-dependent X-ray powder diffraction, has clearly pointed out the unexpected existence of crystalline anhydrous $LaK(C_2O_4)_2$ and $La(NH_4)(C_2O_4)_2$.

ACKNOWLEDGMENT

The authors are indebted to Mr. G. Marsolier for his technical assistance in the collection of powder diffraction data.

REFERENCES

1. V. Kiritsis, A. Michaelides, S. Skoulika, S. Golhen, and L. Ouahab, *Inorg. Chem.* **37,** 3407–3410 (1998).
2. C. Daiguebonne, Y. Gérault, O. Guillou, A. Lecerf, K. Boubekeur, P. Batail, M. Kahn, and O. Kahn, *J. Alloys Compd.* **277,** 50–53 (1998).
3. T. M. Reineke, M. Eddaoudi, M. Fehr, D. Kelley, and O. M. Yaghi, *J. Am. Chem. Soc.* **121,** 1651–1657 (1999).
4. F. Serpaggi, T. Luxbacher, A. K. Cheetham, and G. Férey, *J. Solid State Chem.* **145,** 580–586 (1999).
5. D. Trollet, S. Roméro, A. Mosset, and J.-C. Trombe, *C. R. Acad. Sci. Paris Ser. IIb* **325,** 663–670 (1997).
6. D. M. Y. Barrett Adams, I. A. Kahwa, and J. T. Mague, *New J. Chem.*, 919–921 (1998).
7. T. Bataille, J.-P. Auffrédic, and D. Louër, *Chem. Mater.* **11,** 1559–1567 (1999).
8. D. Louër, *Acta Crystallogr. Sect. A* **54,** 922–933 (1998).
9. J. I. Langford and D. Louër, *Rep. Prog. Phys.* **59,** 131–234 (1996).
10. T. Bataille and D. Louër, *Acta Crystallogr. Sect. C* **55,** 1760–1762 (1999).
11. R. Stella, M. T. Ganzerli Valentini, and L. Maggi, *Appl. Radiat. Isot.* **46,** 1–5 (1995).
12. M. T. Valentini Ganzerli, L. Maggi, and V. Crespi Caramella, *Appl. Radiat. Isot.* **51,** 21–26 (1999).
13. V. C. Caramella, L. Maggi, and M. T. V. Ganzerli, *Appl. Radiat. Isot.* **51,** 353–358 (1999).
14. M. F. Barrett, T. R. R. McDonald, and N. E. Topp, *J. Inorg. Nucl. Chem.* **26,** 931–936 (1964).
15. H. E. Swanson, M. C. Morris, E. H. Evans, and L. Ulmer, "National Bureau of Standards (USA) Monograph 25," Sect. 3, pp. 1–3. Natl. Bur. of Standards, Washington, DC, 1964.
16. A. Boultif and D. Louër, *J. Appl. Crystallogr.* **24,** 987–993 (1991).
17. A. Altomare, M. C. Burla, M. Camalli, B. Carrozzini, G. L. Cascarano, C. Giacovazzo, A. Guagliardi, A. G. G. Moliterni, G. Polidori, and R. Rizzi, *J. Appl. Crystallogr.* **32,** 339–340 (1999).
18. G. M. Sheldrick, "SHELXS-97, Program for the Solution of Crystal Structures; SHELXL-97, Program for Crystal Structure Refinement." University of Göttingen, Göttingen, Germany, 1997.
19. J. Rodriguez-Carvajal, *in* "Collected Abstracts of the Powder Diffraction Meeting, Toulouse, France," pp. 127–128, 1990.
20. W. Kraus and J. Nolze, *J. Appl. Crystallogr.* **29,** 301–303 (1996).
21. J. Plévert, J.-P. Auffrédic, M. Louër, and D. Louër, *J. Mater. Sci.* **24,** 1913–1918 (1989).
22. International Centre for Diffraction Data, Newton Square, PA.
23. A. Altomare, G. Cascarano, C. Giacovazzo, A. Guagliardi, A. G. G. Moliterni, M. C. Burla, and G. Polidori, *J. Appl. Crystallogr.* **28,** 738–744 (1995).
24. I. D. Brown, *J. Appl. Crystallogr.* **29,** 479–480 (1996).
25. W. H. Baur and A. A. Khan, *Acta Crystallogr. Sect. B* **26,** 1584–1596 (1970).
26. W. H. Baur, *Acta Crystallogr. Sect. B* **28,** 1456–1465 (1972).
27. G. Ferraris and M. Franchini-Angela, *Acta Crystallogr. Sect. B* **28,** 3572–3583 (1972).
28. T. R. R. McDonald and J. M. Spink, *Acta Crystallogr.* **23,** 944–949 (1967).
29. M. J. Fuller and J. Pinkstone, *J. Less-Common Met.* **70,** 127–142 (1980).
30. V. Picard, Ph.D. Thesis, Université de Bourgogne, France, 1993.
31. J. O. Sawyer, P. Caro, and L. Eyring, *Monat. Chem.* **102,** 333–354 (1971).
32. G. Pannetier, J. Nataf, and A. Dereigne, *Bull. Soc. Chim. Fr. Ser.* **5,** 318–321 (1965).
33. A.-E. Gobichon, J.-P. Auffrédic, and D. Louër, *Solid State Ionics* **93,** 51–64 (1997).
34. R. P. Turcotte, J. O. Sawyer, and L. Eyring, *Inorg. Chem.* **8,** 238–246 (1969).
35. V. A. Sharov and G. V. Bezdenezhnykh, *Russ. Chem. Rev.* **50,** 630–635 (1981).